Structural Evaluation for Electrodynamic Tape Tethers Against Hypervelocity Space Debris Impacts

Kanjuro Makihara* and Shu Kondo†
Tohoku University, Sendai 980-8579, Japan

DOI: 10.2514/1.A34023

This paper provides a structural evaluation for electrodynamic tape tethers that can resist collisions with small items of space debris. To actively remove space debris such as defunct satellites from orbit, an electrodynamic tether that exploits the interaction between the geomagnetic flux and plasma electrons has been proposed. Among various types of tether, the large width and surface area of tape-shaped designs can resist critical impacts with small items of debris and collect many electrons from plasma space, resulting in successful removal missions. The survival possibility of tether systems in orbital paths evaluates the likelihood of a successful removal mission. In this paper, the relationship between the structural geometries of tape tethers and the impact hole caused by debris impacts is analyzed through large-scale hypervelocity impact experiments. A damage evaluation method based on stress concentration at the impact hole is then proposed to formulate the survivability of tape tethers. Finally, this paper evaluates the survivability of bare tape tethers, enabling comprehensive design guidelines to be identified for improving the survivability. An overall insight into electrodynamic tape tethers should be used for their detailed structural design.

Nomenclature

a	=	major radius of an elliptical hole in a tape tether
B	=	magnetic flux density
b	=	minor radius of an elliptical hole in a tape tether
d	=	diameter of projectile or debris
d_m	=	minimum diameter of debris that may sever a tape tether
d_∞	=	maximum diameter of debris being considered
$F(d)$	=	cumulative flow rate of debris as a function of d
$f_i(\varepsilon)$	=	coefficients of approximate curves as functions of ε (where i is equal to 1, 2, and 3)
f_m	=	scale factor of the minimum debris diameter
H_1, H_2	=	altitudes of target satellite before and after the removal mission, respectively
h	=	thickness of tape tether
I_{av}	=	average current flowing in tape tether
i_{av}	=	coefficient of average current
I_{sc}	=	short circuit current
L	=	length of tether
M_S	=	mass of satellite
$P(t)$	=	survivability of tape tether as a function of t
P_E	=	survivability at the end of debris removal time t_E [equal to $P(t_E)$]
R_E	=	radius of Earth
R_T	=	fatal impact rate (number of debris collisions per unit time)
S	=	cross-sectional area of tape tether
T	=	tensile force
t_E	=	removal time
v	=	velocity of target satellite orbiting in space
W_{eff}	=	effective width
w	=	width of tape tether
$\tilde{w}$	=	minimum width of damaged tether
x_c	=	position of hole center in x direction
α	=	stress concentration factor
α_{dn}	=	stress concentration factor of deep notch
α_{sn}	=	stress concentration factor of shallow notch
Δx_i	=	width of ith strip-shaped segment in x direction
ε	=	ratio of projectile diameter to thickness of tape tether (equal to d/h)
ζ	=	ratio of $2a$ to d (equal to $2a/d$)
η	=	ratio of ρ to $d/2$ (equal to $2\rho/d$)
θ	=	impact angle of debris against tape tether
λ_D	=	Debye length
μ	=	standard gravity parameter (equal to 3.986×10^{14} m^3 s^{-2})
ρ	=	radius of curvature, measured at z equal to zero on the major axis
σ_c	=	critical tensile stress of tether material
σ_{max}	=	maximum tensile stress caused by stress concentration
σ_0	=	tensile stress at infinity (equal to T/S)
$\sigma_{0.2}$	=	0.2% proof stress of tether material
$\tau_i(\sigma_c)$	=	Heaviside unit function for ith segment as a function of σ_c

*Associate Professor, Department of Aerospace Engineering, 6-6-01 Aramaki-Aza-Aoba, Aoba-Ward; makihara@ssl.mech.tohoku.ac.jp. Member AIAA.
†Student, Department of Aerospace Engineering, 6-6-01 Aramaki-Aza-Aoba, Aoba-Ward.

I. Introduction

A. Background on Space Debris

THE amount of space debris around the Earth, especially in the low Earth orbit (LEO), has increased significantly with the development of space exploration [1]. The term "space debris" covers manmade objects such as rocket fairings, defunct artificial satellites, or fragments of satellites resulting from their breakup. The debris travels at high speeds in LEO, and thus has high kinetic energy, which means that even tiny pieces of debris can cause disastrous damage to operational space structures. Debris impacts generate more debris, causing a rapid increase in the total amount of debris. Issues related to space debris were first raised 10 years after the launch of Sputnik 1, with reports considering the intentional and accidental destruction of satellites, as well as accidents caused by collisions with space debris. Space debris represents a serious challenge for the currently operational International Space Station, with actual impact damage reported in 2014 [2]. To date, several destructive collision accidents have taken place in space. In July 1996, the French military reconnaissance satellite "Cerise" collided with a piece of space debris during operation. The colliding debris was refuse from the explosion of the French Ariane rocket 10 years prior. This accident was the first reported collision of an artificial satellite with space debris. In January 2007, a Chinese explosion test with its own weather satellite

(Fengyun 1-C) produced approximately 3000 pieces of observable space debris [3]. In February 2009, an accidental collision occurred between the operational U.S. communications satellite "Iridium 33" and the decommissioned Russian military communications satellite "Kosmos 2251." This accident was the first collision between two artificial satellites in the history of human space development, excluding intentional docking between satellites. The collision generated at least several hundred pieces of debris. In January 2013, the Russian satellite "BLITS" collided with debris from the Chinese explosion tests in 2007, causing the operation of BLITS to be terminated. As of January 2013, 3076 pieces of debris from Fengyun 1-C, 479 pieces of debris from Iridium 33, and 1342 pieces of debris from Kosmos 2251 have been cataloged as being in orbital pathways. The orbital debris from these three satellites alone amounts to approximately 5000 pieces, posing a threat to all operational satellites and space stations [4]. Recent years have seen collisions with small debris and collisions between whole satellites, and the large amount of new space debris generated by these events has resulted in a growing recognition of the seriousness of the debris issue. It has been suggested that the Kessler syndrome [5] (i.e., explosive self-propagation of space debris) will be realized in the near future. Thus, the increased amount of debris is a serious threat to space development, and it is therefore necessary to remove debris, especially from the LEO, in order to continue space activities safely [6–8].

To remove large pieces of debris such as defunct satellites or spent rocket tanks, an electrodynamic tether (EDT; see Fig. 1) [9] shaped like a piece of string has been proposed. The basic concept is to attach the EDT to the target satellite and deorbit the target using the Lorentz force. Electrons are collected from the ambient plasma and are emitted at one end of the EDT, which induces an electric current to flow along the tether. The Lorentz force is caused by the interaction between the current and the Earth's geomagnetic field. This force decelerates the satellite, breaking the balance between centrifugal force and gravity and causing a decrease in the orbital altitude. The removal mission is completed by the reentry and eventual incineration of the satellite in the atmospheric layer. The EDT system is a cost-effective and safe method of removing defunct satellites because it is a lightweight apparatus that requires no chemical propellant. However, the narrow width of the string-shaped tether means it is easily severed by impacts with tiny pieces of debris. The severing of the EDT results in the failure of the removal mission and, instead of eliminating the debris, increases the total amount of debris. It is essential to propose new EDT structures that can endure the impacts of debris: especially tiny debris. Forward et al. [10] of Tethers Unlimited, Inc., proposed the Terminator Tether™, which is a

lightweight, reliable space tether system. Their system greatly reduces debris removal times, and it has triggered further developments in EDT technology. The Inter-Agency Space Debris Coordination Committee documented an action plan [11] for estimating the risk of debris impacts with an EDT during a removal mission. Since then, many research institutions have participated in this plan and developed computational approaches. The survival performance of an EDT is assessed by calculating its survivability; a round tether is easily severed by tiny debris impacts, resulting in low survivability. Pardini et al. [12] and Kim et al. [13] proposed a double tether consisting of multiple loops of wires and knots. In comparison experiments, the double-tether system was shown to have higher survivability than single-tether approaches. Makihara and Takahashi [14] pointed out that the fracture progress of EDTs has not been sufficiently considered in evaluating the survivability, and they investigated the dynamic fracture progress of a round EDT owing to a hypervelocity impact collision with space debris. Kawamoto et al. [15] proposed a net tether consisting of braided tethers made from multiple wires and carbon fibers, and they concluded that this construction would have a long lifetime in orbit. Makihara and Matsumoto [16] proposed a hollow cylindrical mesh tether and determined the severing criteria by conducting hypervelocity impact experiments and numerical simulations. They revealed that the hollow cylindrical tether had higher survivability than conventional tethers. Khan and Sanmartin [17,18] determined the fatal impact rate for tape tethers, and they insisted that a tape tether had a survival probability of about one and one-half orders of magnitude higher than a round tether of equal mass and length.

Among the various shapes that have been proposed, tape-shaped tethers have recently received increased attention because they offer several advantages. The large width of tape-shaped tethers allows them to resist critical impacts with small items of debris, and their large surface areas enable many electrons to be collected from plasma space, resulting in effective removal missions. When a tether is not covered by insulation, it can collect electrons by itself; this is referred to as a bare tether. Sanmartin [19], Sanmartin and Estes [20], and Sanmartin et al. [21] calculated the electrical current flowing along a bare tape tether based on the orbital motion limited (OML) theory. Peláez and Sanjurjo [22] described the main parameters involved in the dynamics of bare tethers and their influence on the balance condition, and they proposed a strategy to keep the tether balanced by taking into account the whole trajectory during the deorbiting process. Bombardelli et al. [23] investigated the deorbiting capability of bare tethers. They employed an eccentric tilted dipole model to compute the deorbiting time with reasonable accuracy. Li and Zhu [24] and Li et al. [25] developed a coupled finite element method (FEM) to analyze the deorbiting of satellites with a bare flexible tether, assuming that the efficiency of electron collection varied depending on tether deflection. Khan and Sanmartin [17,18] theoretically analyzed the correlation between the debris' kinetic energy and the tether damage, and they derived the minimum size of debris that could sever the tape tether. However, they did not prove this using hypervelocity impact experiments. Francesconi et al. [26] conducted impact experiments with tape tethers and spherical projectiles, and they demonstrated the influence of impact angle on hole size. Their experimental study was not sufficient to determine a comprehensive correlation because the tape thickness was not considered. Although some researchers have proposed some tether structures that may improve survivability, hypervelocity impact experiments have not been conducted to prove the superiority of the proposed structures. For the purpose of establishing a reliable design for EDT systems, it is important to determine consistent structural criteria based on hypervelocity impact experiments.

B. Research Objectives

This paper covers three objectives. The first is to reveal the relationship between the geometric dimension of a tape tether and the damage of debris impact. To ensure clarity, large-scale hypervelocity impact experiments are conducted with tape tethers and spherical projectiles. The correlation between the debris diameter, the impact angle of debris, the size of the impact hole, and the thickness of the tape tether is clarified and formulated mathematically.
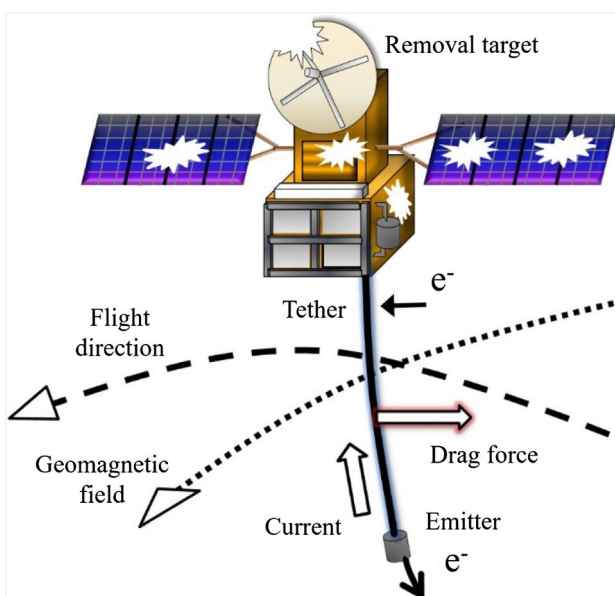
Fig. 1   Debris removal using electrodynamic tether.

The second objective is to propose severing criteria for tape tethers, namely, the criteria that determine whether the tape tethers will be severed by a collision with small debris. The proposed severing criteria are constructed in terms of the tensile stress concentration of the impact hole. A damaged tether with an impact hole may be subjected to tensile force by, for example, attitude control of the EDT system or the gravity gradient between a satellite and an end mass. When a damaged tape tether is pulled, a stress concentration may be generated at the edge of the hole. We propose a damage evaluation method to assess the severing condition of tape tethers after this tensile force is exerted on them. The effective width of the tape tether is also proposed to derive the critical area of the debris' path, which is essential for the survivability evaluation.

The third objective is to evaluate the survivability according to tape dimension and show how the survivability changes with respect to the dimension. The survivability is calculated using the proposed severing criteria and the proposed effective width. Furthermore, this paper provides an assessment of the survivability for bare tape tethers. Survivability assessments with respect to the removal mission time are presented for two cases: a constant cross-sectional area, and a constant thickness.

The remainder of this paper is organized as follows. Section II presents a summary of the hypervelocity impact experiments and their results. Section III explains how the stress concentration is calculated and determines the severing criteria of the tape tethers. Section IV proposes a method for calculating the survivability of tape tethers. A method for calculating the time of debris removal is introduced to consider the survivability of bare tape tethers. Section V presents the survivability calculation results and discusses the subsequent considerations. Section VI describes the conclusions of this paper.

II.   Hypervelocity Impact Experiments

A.   Overview of Hypervelocity Impact Experiments

Hypervelocity impact experiments were conducted by a large-scale instrument: a two-stage light-gas gun [27] (Fig. 2) at the Institute of Space and Astronautical Science/Japanese Exploration Agency (ISAS/JAXA). A high-speed camera (Hyper Vision HPV-X, Shimadzu Corporation) was used to photograph the impact events. The backlight method was employed for the lighting, and photographs were taken at a rate of 500,000 frames per second (frame interval of 2 μs). A spherical aluminum projectile was used to simulate the space debris. The velocity of the projectile was around 7.0 km/s. The experimental cases are summarized in Table 1. The ratio of the projectile diameter d to the tape thickness h is defined as

$$\varepsilon \equiv \frac{d}{h} \qquad (1)$$

Figure 3 shows the fixing apparatus for setting the impact angle of the tether. Multiple tape tethers are arranged in an array so that the projectile collides with one of them. Figure 4 shows a schematic of the impact experiments. The impact angle of the projectiles, expressed as θ, ranges from 0–80 deg. In this study, the projectile moves within the x–y plane because this direction of travel is thought
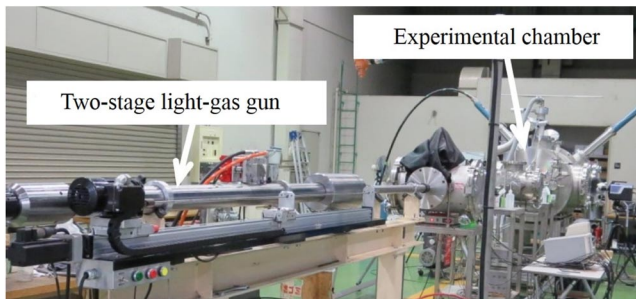

Fig. 2   Two-stage light-gas gun at ISAS/JAXA.

Table 1   Experimental cases of projectile impact

Experiment no.	Width w, mm	Thickness h, mm	Diameter d, mm	Ratio ε (= d/h)	Angle θ, deg
1	12.6	0.15	0.80	5.33	0
2	12.6	0.15	0.80	5.33	30
3	12.6	0.15	0.80	5.33	60
4	12.6	0.15	0.80	5.33	70
5	12.6	0.15	0.80	5.33	80
6	12.6	0.15	0.80	5.33	85
7	12.6	0.15	1.60	10.7	0
8	12.6	0.15	1.60	10.7	30
9	12.6	0.15	1.60	10.7	60
10	12.6	0.15	1.60	10.7	70
11	12.6	0.15	1.60	10.7	80
12	200	0.30	7.90	26.3	0
13	200	0.30	7.90	26.3	30
14	200	0.30	7.90	26.3	60
15	200	0.30	7.90	26.3	70
16	200	0.30	7.90	26.3	80

to provide the most serious damage to tape tethers. The major and minor diameters of the elliptical hole are $2a$ and $2b$, respectively. Figure 5 shows photographs of the typical damage to tape tethers caused by hypervelocity impacts. Figure 5a shows a penetrated hole from experiment no. 12 (normal impact: $\theta = 0$ deg). A precise hole is generated, and the major and minor diameters are equal: $a = b = 2.10$ mm. Figure 5b shows an elliptical hole in experiment no. 8 (oblique impact: $\theta = 30$ deg) with $a = 1.40$ mm and $b = 1.23$ mm.

Figure 5c shows an elliptical hole in experiment no. 3 (oblique impact: $\theta = 60$ deg) with $a = 1.22$ mm and $b = 0.87$ mm. It is natural for oblique impacts to generate elliptical holes. Note that the hole edges generated by hypervelocity impacts are always smooth because the holes are created by the process of melting and solidifying.

B.   Major Diameter of a Hole in the Tape Tether

The ratio ζ of the major diameter of the hole to the projectile diameter is defined as

$$\zeta \equiv \frac{2a}{d} \qquad (2)$$

Figure 6 shows the relationship between ζ, θ, and ε. It is confirmed that ζ increases as θ increases for every value of ε, which is reasonable when we consider that the length of the projection of a projectile with diameter d on the x axis is $d/\cos\theta$. When $\theta = 0$ deg, the experimental case of $\varepsilon = 5.33$ gives the largest value of ζ. However, when $\theta = 80$ deg, the experimental case of $\varepsilon = 26.3$ produces the largest value of ζ. The results also confirm that ζ is affected by ε as well as θ. This agrees with the results reported by Hastings and Garrett [28], who insisted that the damage to a plate was affected by the thickness of the plate. When ε is large (i.e., thinner tether), the temperature hardly rises because the projectile can pass through the tether before there is a sufficient increase in temperature. Thus, it can be observed that the value of a is correlated with the orthogonal projection of the projectiles. The damaged area of the tape tether appears to be equal to the path area of the projectile ($2a \rightarrow d/\cos\theta$) as $\varepsilon \rightarrow \infty$. However, when ε is small (i.e., thicker tether), the temperature rises sharply because the pressure at the point of impact increases rapidly, and this temperature rise melts and vaporizes the projectile and the tether. When ε is small and θ is small, the pressure of the melting and vaporization of tethers leads to large values of a and ζ. When ε is small and θ is large, a projectile obliquely colliding with the thick tether easily breaks up, with one part going up into the upper surface of the tether and the other part going down into the lower surface of the tether. Because of this breakup, the amount of the projectile that passes through the tether decreases and ζ does not increase significantly. The detailed effects of large impact angles ($\theta > 80$ deg) are discussed in Appendix A. To formulate the
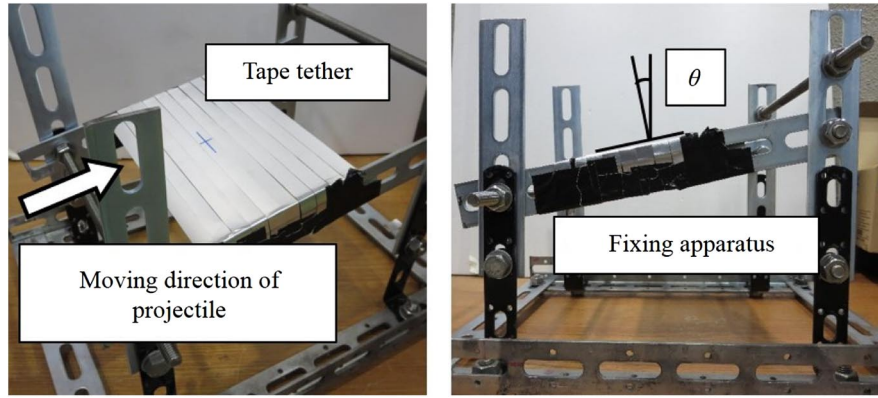
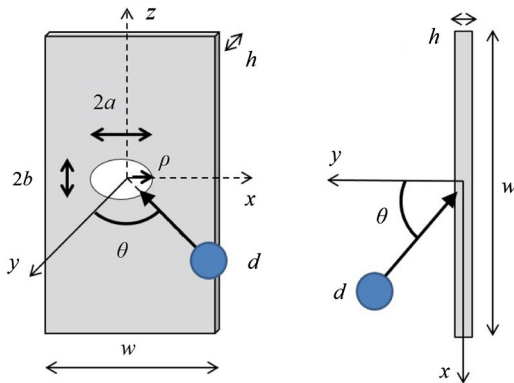Fig. 3 Experimental apparatus to fix tape tethers.

Fig. 4 Schematic illustration of projectile impacting with tape tether.

Fig. 6 Experimental result of ζ as a function of ε and θ.

severing condition of tape tethers in the next section, an approximate equation for ζ is derived from the experimental results in Fig. 6. As the approximate curve of ζ gradually approaches the curve of $1/\cos\theta$ as ε increases, it can be expressed as

$$\zeta(\varepsilon, \theta) = (1 + f_1(\varepsilon))\mathrm{pow}\left[\frac{1}{\cos\theta}, (1 + f_2(\varepsilon))\right] \quad (3)$$

where pow $[X, Y] \equiv X^Y$ is the power function that returns X raised to the power of Y. Here, the two functions $f_1(\varepsilon)$ and $f_2(\varepsilon)$ are perturbation terms reflecting the influence of ε.

C. Radius of Curvature of the Hole in the Tape Tether

The ratio η of the radius of curvature of the hole to the projectile radius is defined as

$$\eta \equiv \frac{\rho}{d/2} = \frac{2\rho}{d} \quad (4)$$

The radius of curvature is measured at $z = 0$ on the major axis (see Fig. 4). Figure 7 shows the relationship between η, θ, and ε. It is confirmed that η decreases as ε and θ increase. The minor diameter b is hardly affected by the impact angle because the direction of movement of the projectile is vertical with respect to the minor radius direction. Thus, b is only influenced by ε. Larger values of ε (i.e., thinner tether) increase a, resulting in small values of ρ and η. Small values of ε and θ lead to circular holes, whereas large values of ε and θ give an elliptical shape. To formulate the severing condition of the
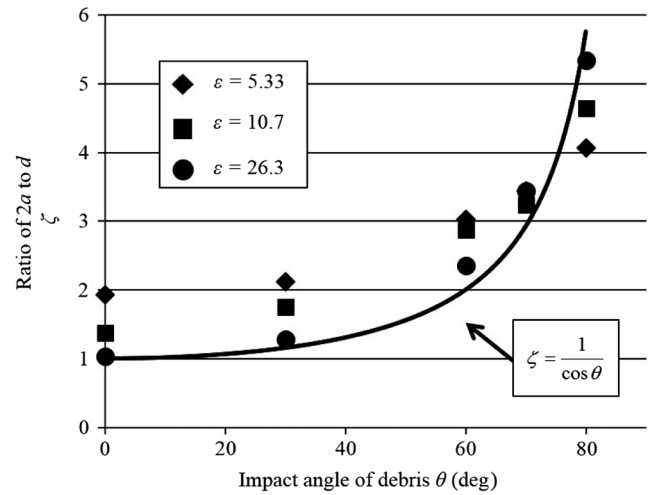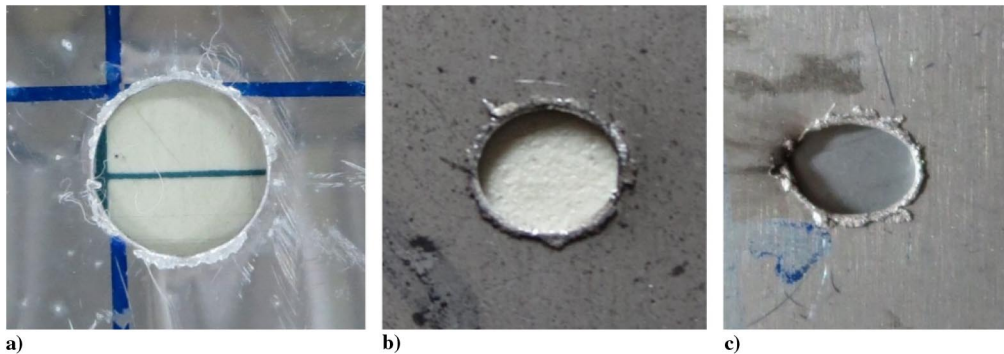

Fig. 5 Impact hole of tape tethers after impact: a) $\theta = 0$ deg and $\varepsilon = 26.3$, b) $\theta = 30$ deg and $\varepsilon = 10.7$, and c) $\theta = 60$ deg and $\varepsilon = 5.33$.
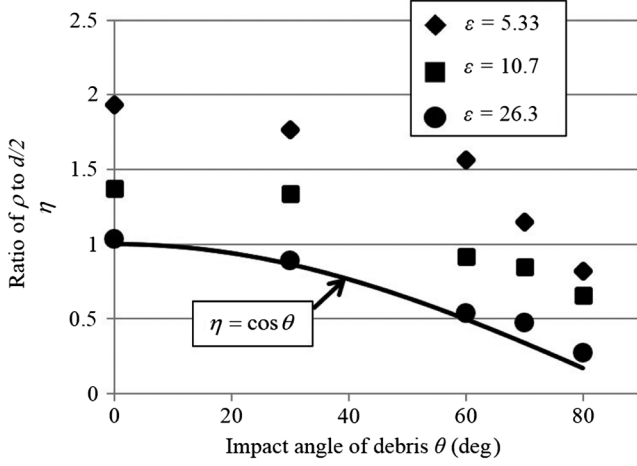
Fig. 7 Experimental result of η as a function of ε and θ.

Fig. 8 Three types of damaged tape tether: a) tape has a notch on one side, b) tape has a hole, and c) tape is separated by a large hole.

tape tether, an approximate equation for η is derived from the experimental results in Fig. 7. The damaged area of the tape is equal to the path area of the projectile $(2a \to d/\cos\theta$ and $2b \to d)$ as $\varepsilon \to \infty$. Because ρ can be expressed as b^2/a, the curve of η gradually approaches the curve of $\cos\theta$ as $\varepsilon \to \infty$. The approximate equation for η is expressed as

$$\eta(\varepsilon, \theta) = (1 + f_1(\varepsilon))\mathrm{pow}[\cos\theta, (1 + f_3(\varepsilon))] \qquad (5)$$

III. Damage Evaluation for Determining the Severing Condition of a Tape Tether

A. Determination by Taking Account of Stress Concentration

In this section, a damage evaluation method for determining the severing condition of tape tethers is proposed. The method is based on the stress concentration at the edge of the hole in the tape tether. There is a chance that small pieces of debris will collide with operational tape tethers, which reduces their structural capability. When the tape tether is hit by a small piece of debris, an impact hole or notch is generated in the tape tether. The damaged tether has less tolerance against tensile force. Tensile force may be generated on the tape tether by the gravity gradient between the satellite and the end mass or by unstable behavior such as swinging or rotation [29,30]. Once in a while during debris removal operations, such tensile forces can be exerted on the tape tether for a short period. The tensile force exerted on a tape tether with a hole or a notch can generate a tensile stress concentration at the edge of the hole. Note that there is little chance of small pieces of debris colliding with the tether while it is being tensioned because both phenomena (i.e., collision and tension) occur only occasionally and for short periods. It is assumed that the tape tether is severed if the maximum stress at the hole edge as a result of this concentration exceeds some critical material-dependent value. In the next subsection, the stress concentration is calculated and compared with the critical stress σ_c to determine whether the tape tether is severed by the tensile force.

B. Calculation of Stress Concentration

The stress concentration describes the local increase in tensile stress inside the material caused by the deformation. When the tensile stress σ_0 is exerted at infinity on the tape tether, the maximum tensile stress at the edge of the hole $\sigma_{\max}$ is

$$\sigma_{\max} \equiv \alpha\sigma_0 \qquad (6)$$

where α is the stress concentration factor [31]. The tape tether is assumed to be severed if the maximum tensile stress $\sigma_{\max}$ exceeds the critical stress σ_c, which is defined as 0.2% proof stress $\sigma_{0.2}$ [32].

There are two reasons to adopt $\sigma_{0.2}$. The first is to calculate the stress concentration with $\sigma_{0.2}$ using only elastic theory rather than
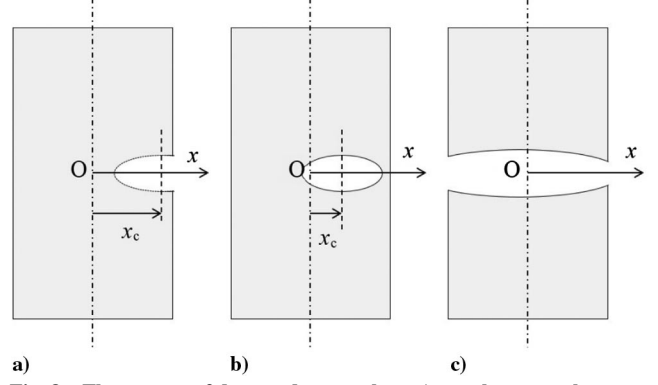
complicated and implicit plastic theories. The second reason is that plastic material is neither safe nor reliable in the space environment, and a tape tether that has full plasticity is not regarded as a proper structure for removal missions. Figure 8 shows three tape tether scenarios regarding the geometry of the impact hole: in Fig. 8a, the tape has a notch on one side in Fig. 8b, the tape has an eccentric hole; and in Fig. 8c, the tape is separated into two halves by a large hole. For each of these scenarios, the maximum stress is calculated. The maximum tensile stress $\sigma_{\max}$ depends on the dimensions of the hole (a, b, and ρ), the position of the hole center x_c, and the tensile stress at infinity σ_0. The dimension of the hole depends on the debris diameter d and the impact angle of the debris θ. The tensile stress depends on the tensile force T and the dimensions of the tape, such as w and h. Thus, the maximum tensile stress $\sigma_{\max}$ is a function of d, h, x_c, T, w, and θ. The explicit expression of the stress is described in detail in Appendix B. The proposed approach based on stress concentration is concise and useful for tailoring the tape because it provides explicit formulations that are advantageous over implicit and complicated FEMs.

C. Impact Position of Debris

The damage and stress concentration vary according to the impact position of the debris, even if the debris diameter and impact angle are the same. To develop a damage evaluation methodology, we consider the virtual impact hole on an imaginary plate that is infinitely wide. The center of the tape tether is located at the origin in the coordinates, and the center location of the virtual hole is x_c in x coordinates, as shown in Fig. 8. Figure 9 shows a schematic of an oblique impact with the tape tether. The elliptical circle (dotted line) is a virtual hole with a major diameter of $2a$. Regarding the trajectory of the debris, there are three impact cases in Fig. 9: in Fig. 9a, the left edge of the debris touches the right edge of the tape; in Fig. 9b, the right edge of the debris touches the left edge of the tape; and in Fig. 9c, the debris passes between both edges of the tape. The case in Fig. 9a leads to $w/2 - a + d/\cos\theta = x_c$, and the case in Fig. 9b leads to $w/2 + a = -x_c$.

When x_c satisfies

$$\frac{w}{2} - a \leq x_c \leq \frac{w}{2} - a + \frac{d}{\cos\theta} \quad \text{or} \quad -\left(\frac{w}{2} + a\right) \leq x_c \leq -\left(\frac{w}{2} - a\right) \qquad (7)$$

the tape tether will become notched, as shown in Fig. 8a. When x_c satisfies

$$-\left(\frac{w}{2} - a\right) < x_c < \frac{w}{2} - a \qquad (8)$$

the tape tether will have an elliptical hole, as shown in Fig. 8b. When $2a > w$ and x_c satisfies Eq. (8), the tape tether becomes separated, as shown in Fig. 8c.
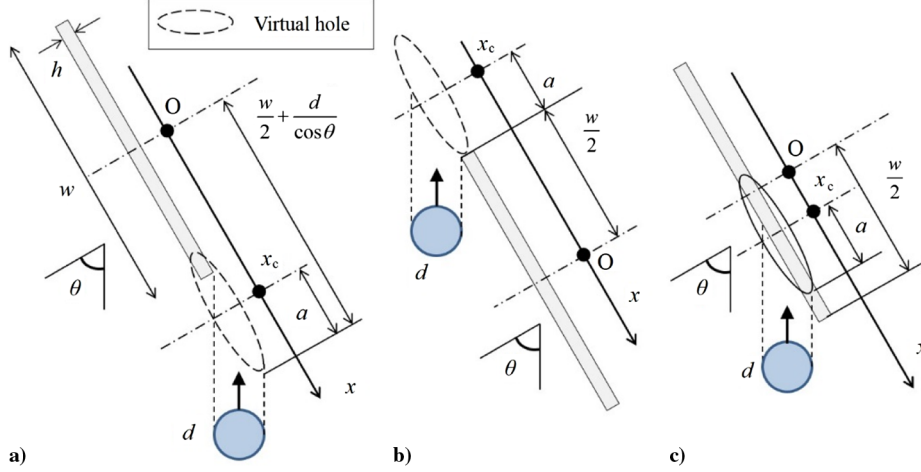
Fig. 9 Oblique impact of debris with tape tether: a) left edge of debris touches right edge of tape tether, b) right edge of debris touches left edge of tape tether, and c) debris passes between both edges of tape tether.
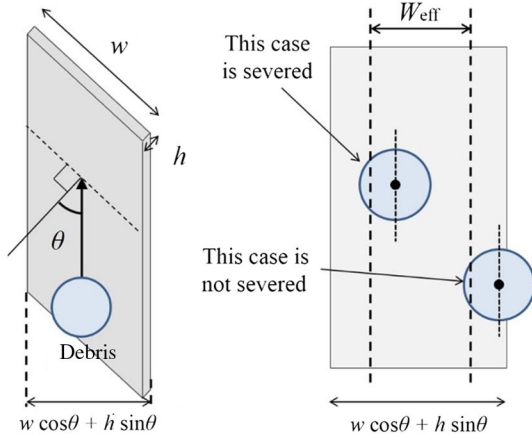

Fig. 10 Schematic illustration of effective width W_{eff}.

Fig. 11 Schematic of strip-shaped segments to determine W_{eff}.

D. Effective Width

We assume that d_m is the minimum diameter of a piece of debris that is able to sever a tether. The orthogonal projection of the tape tether with respect to the direction of the debris flight is considered. The effective width W_{eff} is defined as the width of the area of the tape tether where, if the center of a piece of debris for which the diameter is greater than d_m passes through it, the tether will be severed [12,13]. The left part of Fig. 10 shows the orthogonal projection, and the right shows a schematic of W_{eff}. The strategy for establishing the effective width is to divide the tape tether into a large number $(2N + 1)$ of strip-shaped segments, and then to investigate whether each segment Δx_i is part of W_{eff}. Figure 11 shows a schematic of the method for determining W_{eff}. The effective width W_{eff} is determined by increasing i from $-N$ to N and evaluating the maximum stress on each segment. Thus, W_{eff} is expressed as

$$W_{\mathrm{eff}} \equiv \sum_{i=-N}^{N} \tau_i(\sigma_c)\Delta x_i \cos\theta \qquad (9)$$

where

$$\tau_i(\sigma_c) \equiv \begin{cases} 1 & \text{for} \quad \sigma_c \geq \sigma_{\max} \\ 0 & \text{for} \quad \sigma_c < \sigma_{\max} \end{cases} \qquad (10)$$

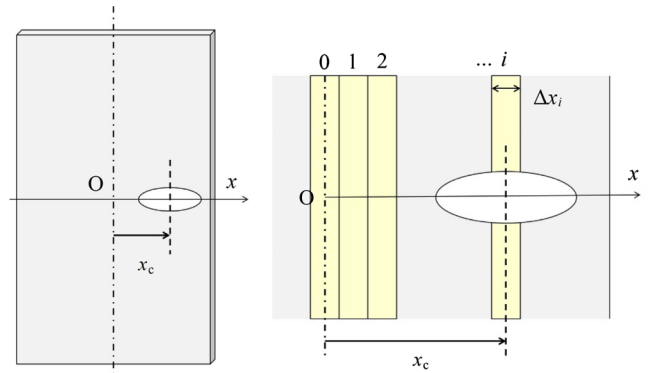If the tape is completely separated into two halves, as shown in Fig. 8c, $\tau_i(\sigma_c)$ is always one.

IV. Calculation of Survival Probability

A. Concept of Survival Probability

The survival probability evaluates the debris removing performance of the tether. The survival probability [12–14,16–18] is defined as the probability that the tether remains intact (i.e., not severed). The probability depends on the tape tether dimensions (width, thickness, and length), debris dimensions (diameter, impact angle, and number), and removal time. NASA's debris flux model ORDEM2000 [33] was used to simulate the cumulative flux of the debris. The debris cumulative flux $F(d)$ is the number of times that debris of a certain diameter d (or greater) pass through a given area of 1 m² in a year. The model is characterized by the altitude, size distribution, and orbital inclination of cataloged debris. Figure 12 shows example data for the cumulative debris flux at an altitude of 800 km and an orbital inclination of 28.5 deg.

B. Removal Time of Bare Tape Tether

Plasma consisting of electrons and ions is created by the solar wind or atmospheric ionization under ultraviolet light. A bare tether can collect electrons from ambient plasma anywhere on the tether surface. An electric current (i.e., the movement of electrons) is generated inside the electrodynamic tether by the work of an emitter. Sanmartin et al. [19], Sanmartin and Estes [20], and Sanmartin et al. [21] presented the operational principles of bare tape tethers using the OML theory. According to this theory, the average current I_{av} flowing inside the bare tape tether is

$$I_{\mathrm{av}} = i_{\mathrm{av}}(\xi)I_{\mathrm{sc}}, \qquad \xi \equiv \frac{L}{h^{2/3}l^{1/3}} \qquad (11)$$
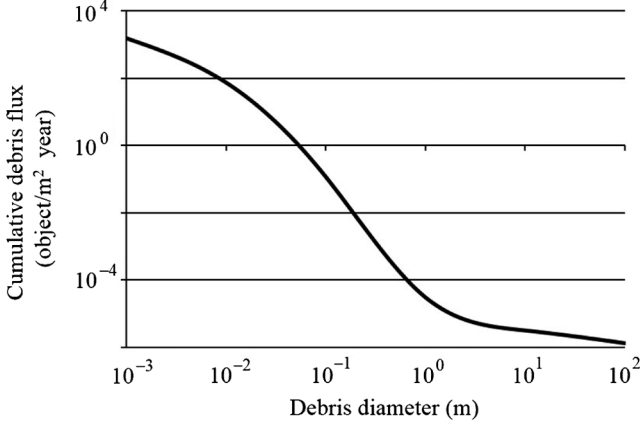
Fig. 12 Cumulative debris flux vs debris diameter curve.

The functions $i_{av}(\xi)$, I_{sc}, and l were defined in [19–22,24,25]. An OML current is generated if the tape tether satisfies

$$w \leq 4\lambda_D \tag{12}$$

where λ_D is the Debye length [19–22,24,25]. We assume that a satellite travels in quasi-circular orbits at an altitude of H, and the variation of H is quite slow. The equation of motion for the target satellite and the tether system can be expressed as

$$M_S \frac{dv}{dt} = I_{av} B L \tag{13}$$

where $I_{av}BL$ is the Lorentz force. By substituting $v^2 = \mu/(R_E + H)$ into Eq. (13), we obtain

$$t_E = \int_0^{t_E} dt = -\int_{H_1}^{H_2} \frac{M_S \sqrt{\mu}}{2 I_{av} BL} (R_E + H)^{-(3/2)} \, dH \tag{14}$$

With the assumption that I_{av} and B are constant between H_1 and H_2, the removal time t_E is obtained as

$$t_E = \frac{M_S}{I_{av} BL} \sqrt{\frac{\mu}{R_E}} \left[\left(1 + \frac{H_2}{R_E} \right)^{-(1/2)} - \left(1 + \frac{H_1}{R_E} \right)^{-(1/2)} \right] \tag{15}$$

C. Formulation of Survival Probability for Tape Tether

A tape tether of length L has an effective area of LW_{eff}. If the center of debris passes within this area, the tape tether is severed. The number of pieces of debris that may pass within this area during a year, defined as R_T [17,18], is expressed as

$$R_T \equiv -\frac{2}{\pi} \int_0^{\pi/2} \int_{d_m}^{d_\infty} LW_{eff} \frac{dF(d)}{dd} \, dd \, d\theta \tag{16}$$

where d_∞ is the maximum debris diameter provided by the ORDEM2000 debris flux model. The minimum debris diameter d_m is given by $f_m(w \cos \theta + h \sin \theta)$, where f_m is the scale factor [17]. The variation of d_m for highly oblique impacts is neglected in this study. According to [12–14,16], the survivability $P(t)$ is obtained as

$$P(t) = \exp(-R_T t) \tag{17}$$

V. Evaluation Results for Survivability

A. Evaluation Condition

Let us consider how the survivability is affected by the cross-sectional area, thickness, and length of tape tethers. For a fair comparison, the mass of the tape tethers is assumed to be constant (20 kg). Table 2 describes four examples of tape tethers with a thickness of $h = 0.10$ mm, and Table 3 describes four cases of tape tethers with a cross-sectional area of $S = 1.0$ mm². A regression

analysis is used to determine the functions in Eqs. (3) and (5) (see Table 4). Note that regression functions formulated in various ways offer a compromise between fidelity and simplicity. We set $\sigma_c = 170$ N/mm² for aluminum: a material that is commonly used in space developments. A large cross-sectional area increases the number of pieces of debris that may pass within the critical area during a year, but García-Pelayo et al. [34] concluded that multiple impacts of very small particles on a tape tether did not make a great difference in terms of survivability. Thus, in this study, we neglect the effect of damage from multiple impacts.

B. Survivability of Bare Tape Tethers

The removal time of bare tethers is affected by the tether dimensions. The survivability for bare tethers is evaluated by taking account of the removal time. It is assumed that the tape tether system deorbits a satellite of 4000 kg from an altitude of 800 to 300 km. The survivability is calculated based on the scenario introduced in [14,17]. The cumulative debris flux is that shown in Fig. 12 (altitude = 800 km, orbital inclination = 28.5 deg, year = 2000). The mass of the aluminum tape tether is restricted to 20 kg. The geomagnetic flux B is 4.60×10^{-5} T, which is the average observed value. In Eq. (16), f_m is set to $1/3$ and d_∞ is set to 1 m [17]. Figure 13 shows the contour plot of the removal time as a function of the thickness and cross-sectional area of the tape tethers. The top, left area in the figure has not been drawn because the combination of thickness and cross-sectional area does not meet the criteria of Eq. (12). Here, there are two conflicting factors for the removal performance of tape tethers. The first is that the length of a tether is shorter when the cross-sectional area is larger. Thus, the average current is larger because of the decrease in electric resistance, which may lead to effective removal performance. The second factor is that the Lorentz force is smaller when the cross-sectional area is larger because of the shorter tether length. Thus, the large cross-sectional area may lengthen the removal time. The removal time may be affected by the cross-sectional area and thickness of the tape tethers.

The four tape tethers described in Table 2 are compared. The final survivability at the overall debris removal time t_E is defined as $P_E (= P(t_E))$. The removal times for four cases (from a-1 to a-4) are 52, 57, 66, and 75 days, respectively. Figure 14 shows the time history of the survivability of tape tethers (Table 2) under a tensile force of 10 N. The number of days in the figure indicates the removal time t_E.

Table 2 Four simulation cases of tape tethers (thickness is constant)

Case no.	w, mm	h, mm	S, mm²	L, km
a-1	7.00	0.10	0.70	10.5
a-2	10.0	0.10	1.00	7.33
a-3	14.0	0.10	1.40	5.23
a-4	18.0	0.10	1.80	4.07

Table 3 Four simulation cases of tape tethers (cross-sectional area is constant)

Case no.	w, mm	h, mm	S, mm²	L, km
b-1	20.0	0.05	1.00	7.33
b-2	10.0	0.10	1.00	7.33
b-3	6.67	0.15	1.00	7.33
b-4	5.00	0.20	1.00	7.33

Table 4 Functions in regression analysis

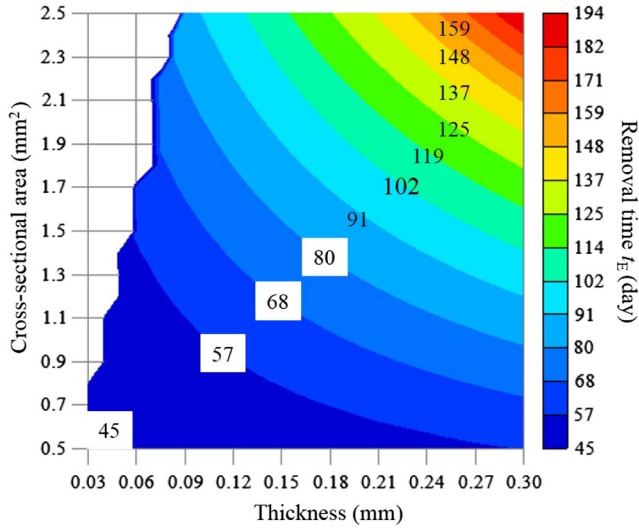| Name	Functions
$f_1(\varepsilon)$	$1.98 \exp(-1.5 \times 10^{-1} \varepsilon)$
$f_2(\varepsilon)$	$-1.02 \exp(-1.2 \times 10^{-1} \varepsilon)$
$f_3(\varepsilon)$	$-0.638 \exp(-1.96 \times 10^{-2} \varepsilon)$

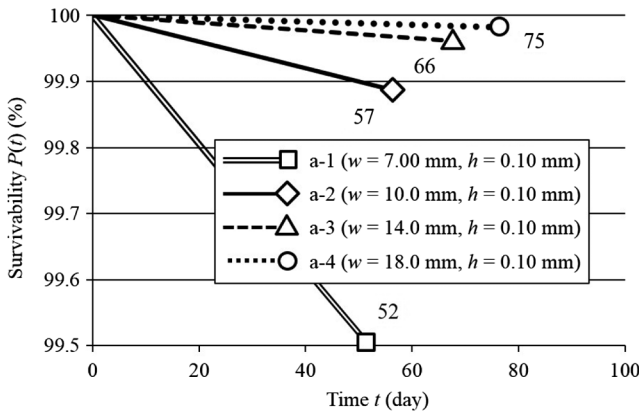**Fig. 13 Contour plot of removal time as a function of thickness and cross-sectional area.**

Fig. 14 Survivability of bare tape tethers with $T = 10$ N (thickness is constant).

Tape a-1 has the shortest removal time but the lowest final survivability. In contrast, tape a-4 has the longest removal time but the highest final survivability. These results may contradict our expectations because we tend to think that a short removal time implies higher survivability. It has been confirmed that, within a reasonable range, a large cross-sectional area can improve P_E in bare tape tethers, even though the removal time is relatively long.

The four tape tethers described in Table 3 are now compared. Figure 15 shows the relationship between the time and survivability of
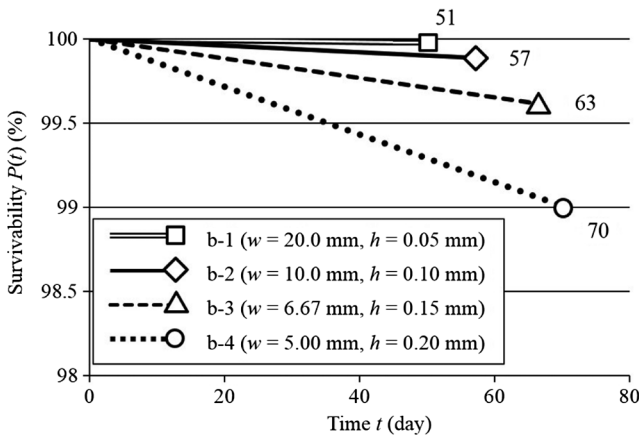

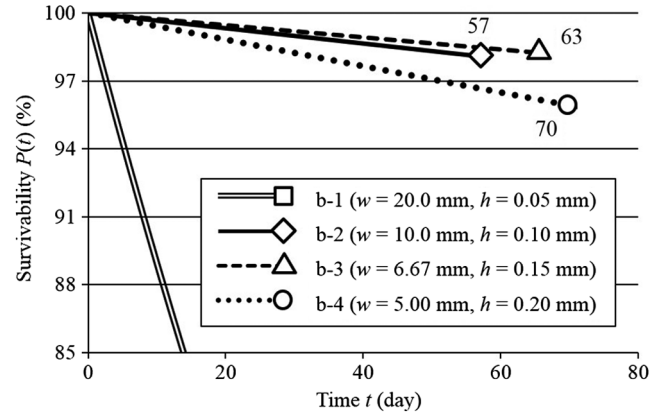**Fig. 15 Survivability of bare tape tethers with $T = 10$ N (cross-sectional area is constant).**

Fig. 16 Survivability of bare tape tethers with $T = 30$ N (cross-sectional area is constant).

the bare tape tethers (Table 3) under a tensile force of 10 N. Tape b-1 has the longest final survivability. Small thickness values result in improved final survivability. Tape b-1 has the shortest removal time and the highest final survivability, which is clearly the best overall performance. Figure 16 shows the time history of the survivability of the bare tape tethers (Table 3) under a tensile force of 30 N. Tape b-3 has the highest survivability, whereas b-1 has the lowest. The superiority order of the overall survivability is different in Figs. 15 and 16. As will be discussed in the next subsection, the tensile force is an important factor in evaluating the final survivability. We can conclude that the final survivability strongly depends on both the removal time and the tensile force, and so both factors must be considered in the design of tape tethers. Sanmartin et al. [21] discussed the relation between the removal time and the tether geometries, concluding that the removal time depended on $L/h^{2/3}$ and the dimensionless function that was proportional to $R_T t_E$ depended weakly on h and had a minimum value that was a function of $L/h^{2/3}$. A comparison of the results of the present study with those in [21] indicates that the effect of impact holes on survivability, as discussed in this paper, provides new insights into the structural design of tape tethers.

C. Design Guidelines for Improving the Final Survivability of Tape Structures

Figure 17 shows the relationship between the tensile force T and final survivability P_E of bare tethers (Table 2) of constant thickness. This relation includes the influence of removal time on final survivability. The final survivability of tape a-1, which has the smallest cross-sectional area, decreases sharply at around 20 N. The final survivability of tape a-4, which has the largest cross-sectional area, decreases sharply above 50 N. When the tensile force is large, the tape tether is easily severed by even small holes. The number of impact holes increases as the tensile force becomes larger, which leads to a
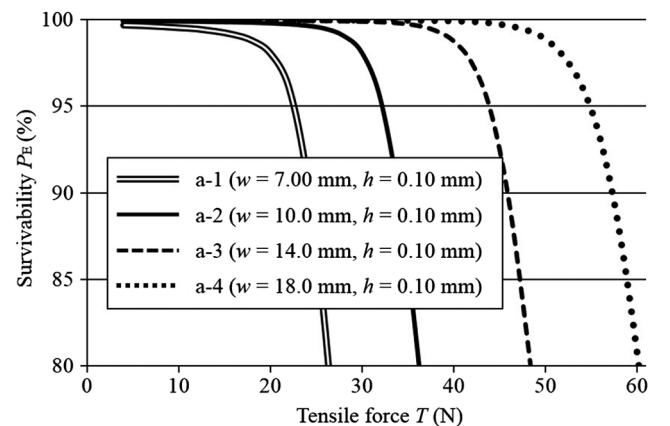

Fig. 17 Final survivability of bare tape tethers (thickness is constant).
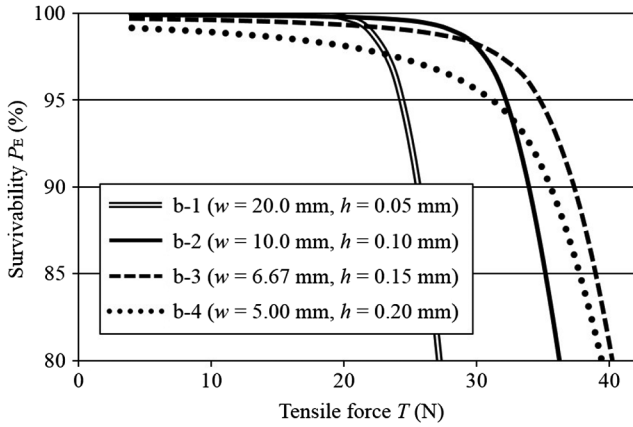
Fig. 18   Final survivability of bare tape tethers (cross-sectional area is constant).

sharp drop in the final survivability. Figure 18 shows the relationship between the tensile force and the final survivability of bare tethers (Table 3) of constant cross-sectional area. Tape b-1 has the highest final survivability when the tensile force is less than 20 N. For tensile forces of 20–30 N, tape b-2 has the highest survivability. At tensile forces greater than 30 N, tape b-3 has the highest final survivability. The value of P_E varies significantly over this range of tensile force. For the purpose of effective tape tether design, we need to consider a range of tensile forces to evaluate the final survivability of tape tethers.

One approach for improving the final survivability is to increase the cross-sectional area of tape tethers: even those of short length, as can be seen in Fig. 17. It is possible to decrease σ_0 by increasing the cross-sectional area, leading to a decrease in σ_{max} at the edge of the hole. Thus, larger cross-sectional areas can attenuate the stress concentration, resulting in high final survivability. Another approach to improve the final survivability is to adjust the thickness of the tape tether to the possible tensile force. We can now draw an interesting conclusion on the design of tape tethers in Fig. 18. When the tensile force is small, a small tape thickness and large width can improve the survivability. On the contrary, when the tensile force is large, only the thickness should be increased. Therefore, under the restricted condition of tape tethers, an adequate thickness and width can dramatically improve the survivability. Thus, the results presented in this paper offer effective design guidelines for improving the survivability of tape tethers.

Based on the results presented in this paper, we developed sophisticated tape tethers to enhance the survival probability of an EDT system. The superiority of these tape tethers is expected to contribute to the success of EDT missions in removing space debris, and thus help accelerate space development. Furthermore, the tape tether design presented in this paper can theoretically be applied to the design of gravity-gradient tapes [8] and the construction of a space elevator using thin and long tethers.

VI.   Conclusions

This paper provides an overall insight into structural aspects of electrodynamic tape tethers. Tape-shaped tethers can resist critical impacts from small pieces of debris because of their large width, and they can collect many electrons from plasma space because of their large surface area, resulting in effective removal missions. Thanks to their structural properties, these tape tethers are expected to increase survival probabilities during removal operations.

Hypervelocity impact experiments were conducted using a large-scale device. The relationship between the structural geometries of tape tethers and the impact holes caused by debris was analyzed, and it was observed that oblique impacts generated elliptical holes for which the size depended on the tape thickness as well as the diameter and impact angle of the projectiles. In particular, the major diameter and radius of curvature of the hole were affected by the ratio of the debris diameter to the thickness of the tape, as well as the impact angle.

A damage evaluation method based on the stress concentration at the impact hole was proposed to formulate the survivability of a tape tether.

The evaluation method calculated the maximum stress around the hole and compared this with the critical stress. It was confirmed that the proposed method could determine whether the tape tether would be severed or not during the debris removal period. To establish the survivability evaluation, the effective width was determined by taking account of the method using the stress concentration and maximum stress.

This paper has evaluated the survivability of bare tape tethers to establish comprehensive design guidelines for improving their survivability. It was confirmed that the survivability depended on the tensile force, thickness, and cross-sectional area of the tape tether. For a tape tether of constant mass, a large cross-sectional area could improve the survivability. The small thickness increased the survivability when the tensile force was small, whereas large thicknesses could increase the survivability when the tensile force was large. As a result, it was confirmed that the thickness and cross-sectional area of the tape should be carefully considered in determining the structural design of such tethers.

Appendix A: XXXX

This appendix discusses oblique impacts with a large impact angle ($\theta > 80$ deg). Figure A1 shows an experimental image captured by the high-speed camera with the image-capturing method [A1]. The generated debris cloud spreads up and down, and the size of the upper cloud increases as θ becomes larger. Francesconi et al. [A2] discussed the fragmentation of debris on impact at highly oblique angles. They reported that the velocity component normal to the tape became small with increasing impact obliquity and debris pieces bounced along the tape. Christiansen et al. [A3] conducted oblique impact experiments on thick plates and revealed that the maximum depth of the impact hole decreased as θ became larger. In particular, when $\theta > 80$ deg, the maximum depth was quite small. Taking this into account, the perforation energy of the projectile was expected to decrease as θ increased. When θ reached nearly 90 deg, the projectile had difficulty in perforating the tape tether. In fact, the projectile did not perforate the tape tether when $\varepsilon = 5.33$ and $\theta = 85$ deg. Hence, the impact case where θ exceeded 80 deg was not considered in this paper.

Appendix B: XXXX

This appendix derives the explicit formulation for calculating the stress concentration in the three scenarios in Fig. 8. The methods of Neuber [B1] and Luo et al. [B2] are adopted to analytically evaluate the stress concentration in the damaged tape tethers.

B.1.   When the Tape Has a Notch

Figure B1 shows a schematic illustration of the tape tether with a notch. The notch is referred to as a "deep notch" when $\tilde{w}$ is less than ρ, whereas it is referred to as a "shallow notch" when $\tilde{w}$ is greater than ρ. The stress concentration factor of an arbitrary deep notch is expressed by interpolating between the factor of a deep notch α_{dn} and the factor of a shallow notch α_{sn}. Thus, the maximum stress $\sigma_{max,A}$ is given by [B1]
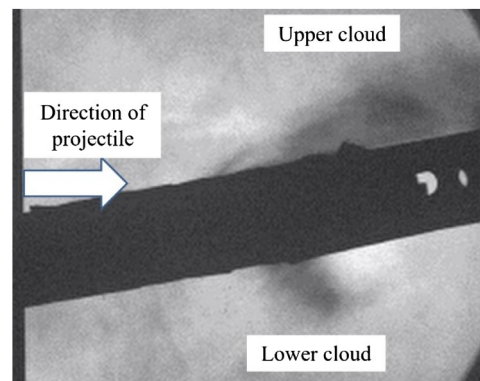

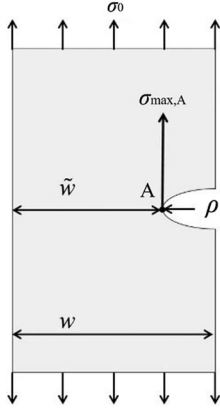**Fig. A1   Image of oblique impact (80 deg) to tape tether.**

Fig. B1   Dimensions to evaluate stress concentration.

Fig. B2   Approximate solution of stress concentration for an eccentric hole.

$$\sigma_{\max,A} = \left(1 + \frac{(\alpha_{\mathrm{dn}}-1)(\alpha_{\mathrm{sn}}-1)}{\sqrt{(\alpha_{\mathrm{dn}}-1)^2(\alpha_{\mathrm{sn}}-1)^2}}\right)\sigma_0 \tag{B1}$$

where

$$\alpha_{\mathrm{dn}} \equiv \frac{w}{\tilde{w}}\frac{\alpha_1 - 2C}{1-(C/\sqrt{\tilde{w}/\rho+1})},$$

$$\alpha_{\mathrm{sn}} \equiv 1 + 2\sqrt{\frac{w-\tilde{w}}{\rho}},$$

$$C \equiv \frac{\alpha_1 - \sqrt{(\tilde{w}/\rho)+1}}{(4/3\alpha_2)\sqrt{(\tilde{w}/\rho)+1}-1},$$

$$\alpha_1 \equiv \frac{2((\tilde{w}/\rho)+1)\sqrt{(\tilde{w}/\rho)}}{((\tilde{w}/\rho)+1)\tan^{-1}\sqrt{(\tilde{w}/\rho)}+\sqrt{(\tilde{w}/\rho)}},$$

$$\alpha_2 \equiv \frac{4(\tilde{w}/\rho)\sqrt{(\tilde{w}/\rho)}}{3\{\sqrt{(\tilde{w}/\rho)}+((\tilde{w}/\rho)-1)\tan^{-1}\sqrt{(\tilde{w}/\rho)}\}} \tag{B2}$$

B.2.   When the Tape Has an Eccentric Hole

Figure B2 shows a schematic illustration of the tape tether with an eccentric elliptical hole. When $x_c > 0$, the stress at point B exceeds the stress at point A. First, we check whether $\sigma_{\max,B}$ exceeds σ_c. The maximum stress at point B is given by [B2]

$$\sigma_{\max,B} = \frac{Z_+}{Y_- Z_+ + Y_+ Z_-}\left(1 + 2\frac{a}{b}\right)\sigma_0 \tag{B3}$$

It is assumed that, if $\sigma_{\max,B} \geq \sigma_c$, cross-section BB' is severed due to the crack propagation of thin tethers. After cross-section BB' has been severed, cross-section AA' receives all of the tensile load. To calculate a new maximum stress at point A $\sigma_{\max,A}$, the hole is approximated as a notch with the same radius of curvature, as shown in Fig. B2. Then, $\sigma_{\max,A}$ is obtained in a similar manner as for case (a). Cross-section AA' is severed if $\sigma_{\max,A} \geq \sigma_c$.

B.3.   When the Tape is Separated into Two Halves by a Large Hole

The tape is severed completely and cannot receive any tensile load.

Acknowledgments

References

[1] Pelton, J. N., *Space Debris and Other Threats from Outer Space*, Springer-Verlag, New York, 2013, pp. 17–44.
[2] "XXXX," *Orbital Debris Quarterly News*, Vol. 18, No. 4, 2014, pp. 3–4.
[3] "XXXX," *Orbital Debris Quarterly News*, Vol. 14, No. 3, 2010, pp. 2–3.
[4] "XXXX," *Orbital Debris Quarterly News*, Vol. 17, No. 1, 2013, pp. 1–6.

$$Y_{\pm} \equiv \frac{((b^2/2)-ab)((w/2)\pm x_c)+(a^2-ab+(b^2/2))\sqrt{((w/2)\pm x_c)^2-\beta}+((a-b)b^3/2\sqrt{((w/2)\pm x_c)^2-\beta})}{w(a-b)^2} \tag{B4}$$

$$\begin{aligned}
Z_{\pm} \equiv &\frac{b^2((w/2)\pm x_c)}{(a-b)^2}\\
&+\frac{(((w/2)\pm x_c)^2(a^2-2ab)-a(a^3-2a^2b+b^3))x_c}{(a-b)^2\sqrt{((w/2)\pm x_c)^2-\beta}}\\
&+\frac{b^2((w/2)\pm x_c)^2+a^2b^2(a-b)}{2(a-b)^2}\\
&-\frac{((w/2)\pm x_c)^3a(2b-a)+((w/2)\pm x_c)a^2(a-b)^2}{2(a-b)^2\sqrt{((w/2)\pm x_c)^2-\beta}}\\
&+\frac{a^2}{2}\log\left(\frac{(w/2)-x_c+\sqrt{((w/2)\pm x_c)^2-\beta}}{a+b}\right), \quad \beta\equiv a^2-b^2
\end{aligned} \tag{B5}$$

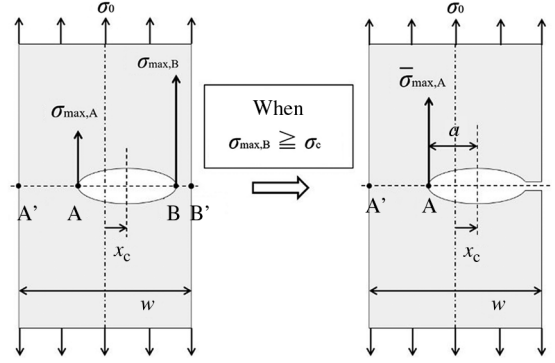[5] Kessler, D. J., "Collisional Cascading: The Limits of Population Growth in Low Earth Orbit," *Advances in Space Research*, Vol. 11, No. 12, 1991, pp. 63–66.
doi:10.1016/0273-1177(91)90543-S
[6] Shan, M., Guo, J., and Gill, E., "Review and Comparison of Active Space Debris Capturing and Removal Methods," *Progress in Aerospace Sciences*, Vol. 80, Jan. 2016, pp. 18–32.
doi:10.1016/j.paerosci.2015.11.001
[7] Macdonald, M., McInnes, C., Bewick, C., Visagie, L., Lappas, V., and Erb, S., "Concept-of-Operations Disposal Analysis of Spacecraft by Gossamer Structure," *Journal of Spacecraft and Rockets*, Vol. 52, No. 2, 2015, pp. 517–525.
doi:10.2514/1.A32919
[8] Nock, K. T., Aaron, K. M., and McKnight, D., "Removing Orbital Debris with Less Risk," *Journal of Spacecraft and Rockets*, Vol. 50, No. 2, 2013, pp. 365–379.
doi:10.2514/1.A32286

[9] Cosmo, M. L., and Lorenzini, E. C., *Tethers in Space Handbook*, 3rd ed., Smithsonian Astrophysical Observatory, Cambridge, MA, 1997, pp. 137–151.

[10] Forward, R. L., Hoyt, R. P., and Uphoff, C. W., "Terminator Tether™: A Spacecraft Deorbit Device," *Journal of Spacecraft and Rockets*, Vol. 37, No. 2, 2000, pp. 187–196.
doi:10.2514/2.3565

[11] Beltrami, P., "Comparison of Debris Flux Models," Inter-Agency Space Debris Coordination Committee Final Rept. of Action Item 19.2, Document IADC- 05-03, 2005.

[12] Pardini, C., Hanada, T., and Krisko, P. H., "Benefits and Risks of Using Electrodynamic Tethers to De-Orbit," *Acta Astronautica*, Vol. 64, Nos. 5–6, 2009, pp. 571–588.
doi:10.1016/j.actaastro.2008.10.007

[13] Kim, I., Hirayama, H., and Hanada, T., "Practical Guidelines for Electro-Dynamic Tethers to Survive from Orbital Debris Impacts," *Advances in Space Research*, Vol. 45, No. 10, 2010, pp. 1292–1300.
doi:10.1016/j.asr.2010.01.012

[14] Makihara, K., and Takahashi, R., "Survivability Evaluation of Electrodynamic Tethers Considering Dynamic Fracture in Space-Debris Impact," *Journal of Spacecraft and Rockets*, Vol. 53, No. 1, 2016, pp. 209–216.
doi:10.2514/1.A33328

[15] Kawamoto, S., Makida, T., Sasaki, F., Okawa, Y., and Nishida, S., "Precise Numerical Simulations of Electrodynamic Tethers for an Active Debris Removal System," *Acta Astronautica*, Vol. 59, Nos. 1–5, 2006, pp. 139–148.
doi:10.1016/j.actaastro.2006.02.035

[16] Makihara, M., and Matsumoto, N., "Survival Probability of Hollow Cylindrical Mesh Tether Under Space Debris Impact," *Journal of Spacecraft and Rockets*, Vol. 53, No. 3, 2016, pp. 520–527.
doi:10.2514/1.A33379

[17] Khan, S. B., and Sanmartin, J. R., "Survival Probability of Round and Tape Tethers Against Debris Impact," *Journal of Spacecraft and Rockets*, Vol. 50, No. 3, 2013, pp. 603–608.
doi:10.2514/1.A32383

[18] Khan, S. B., and Sanmartin, J. R., "Analysis of Tape Tether Survival in LEO Against Orbital Debris," *Advances in Space Research*, Vol. 53, No. 9, 2014, pp. 1370–1376.
doi:10.1016/j.asr.2014.02.008

[19] Sanmartin, J. R., Martinez-Sánchez, M., and Ahedo, E., "Bare Wire Anodes for Electrodynamic Tethers," *Journal of Propulsion and Power*, Vol. 9, No. 3, 1993, pp. 353–360.
doi:10.2514/3.23629

[20] Sanmartin, J. R., and Estes, R. D., "The Orbital-Motion-Limited Regime of Cylindrical Langmuir Probes," *Physics of Plasmas*, Vol. 6, No. 1, 1999, pp. 395–405.
doi:10.1063/1.873293

[21] Sanmartin, J. R., Sánchez-Torres, A., Khan, S. B., Sánchez-Arriaga, G., and Charro, M., "Optimum Sizing of Bare-Tape Tethers for De-Orbiting Satellite at End of Mission," *Advances in Space Research*, Vol. 56, No. 7, 2015, pp. 1485–1492.
doi:10.1016/j.asr.2015.06.030

[22] Peláez, J., and Sanjurjo, M., "Generator Regime of Self-Balanced Electrodynamic Bare Tethers," *Journal of Spacecraft and Rockets*, Vol. 43, No. 6, 2006, pp. 1359–1369.
doi:10.2514/1.20471

[23] Bombardelli, C., Zanutto, D., and Lorenzini, E., "Deorbiting Performance of Bare Electrodynamic Tethers in Inclined Orbits," *Journal of Guidance, Control, and Dynamics*, Vol. 36, No. 5, 2013, pp. 1550–1556.
doi:10.2514/1.58428

[24] Li, G., and Zhu, Z. H., "Multiphysics Finite Element Modeling of Current Generation of Bare Flexible Electrodynamic Tether," *Journal of Propulsion and Power*, Vol. 33, No. 2, 2017, pp. 408–419.
doi:10.2514/1.B36211

[25] Li, G., Zhu, Z. H., Ruel, S., and Meguid, S. A., "Multiphysics Elastodynamic Finite Element Analysis of Space Debris Deorbit Stability and Efficiency by Electrodynamic Tethers," *Acta Astronautica*, Vol. 137, Aug. 2017, pp. 320–333.
doi:10.1016/j.actaastro.2017.04.025

[26] Francesconi, A., Giacomuzzo, C., and Lorenzini, E. C., "Survivability to Hypervelocity Impacts of Electrodynamic Tape Tethers for Deorbiting Spacecraft in LEO," *6th European Conference on Space Debris*, ESA SP-723, Darmstadt, Germany, April 2013.

[27] Kawai, N., Tsurui, K., Hasegawa, S., and Sato, E., "Single Microparticle Launching Method Using Two-Stage Light-Gas Gun for Simulating Hypervelocity Impacts of Micrometeoroids and Space Debris," *Review of Scientific Instruments*, Vol. 81, No. 11, 2010, Paper 115105.
doi:10.1063/1.3498896

[28] Hastings, D., and Garrett, H., *Spacecraft-Environment Interactions*, Cambridge Univ. Press, Cambridge, England, U.K., 2004.

[29] Mantri, P., Mazzoleni, A. P., and Padgett, D. A., "Parametric Study of Deployment of Tethered Satellite Systems," *Journal of Spacecraft and Rockets*, Vol. 44, No. 2, 2007, pp. 412–423.
doi:10.2514/1.22955

[30] Jung, W., Mazzoleni, A. P., and Chung, J., "Dynamic Analysis of a Tethered Satellite System with a Moving Mass," *Nonlinear Dynamics*, Vol. 75, Nos. 1–2, 2014, pp. 267–281.
doi:10.1007/s11071-013-1064-8

[31] Timoshenko, S., and Goodier, J. N., *Theory of Elasticity*, 2nd ed., Maple Press, York, PA, 1951, pp. 78–85.

[32] Case, J., Chilver, L., and Ross, C. T. F., *Strength of Materials and Structures, with an Introduction to Finite Element Methods*, 3rd ed., Edward Arnold, London, 1993, pp. 10–46.

[33] Liou, J.-C., Matney, M. J., Anz-Meador, P. D., Kessler, D., Jansen, M., and Theall, J. R., "The New NASA Orbital Debris Engineering Model ORDEM2000," NASA/ TP-2002-210780, 2002.

[34] García-Pelayo, R., Khan, S. B., and Sanmartin, J. R., "Survivability Analysis of Tape-Tether against Two Concurring Impacts with Debris," *Advances in Space Research*, Vol. 57, No. 11, 2016, pp. 2273–2284.
doi:10.1016/j.asr.2016.03.018

[35] Makihara, K., and Oki, Y., "Bayesian Cloud Extraction for Assessment of Space-Debris Impact Using Conditional Entropy," *Journal of Spacecraft and Rockets*, Vol. 54, No. 6, 2017, pp. 1235–1245.

[36] Francesconi, A., Giacomuzzo, C., Bettiol, L., and Lorenzini, E., "A New Ballistic Limit Equation for Thin Tape Tethers," *Acta Astronautica*, Vol. 129, Dec. 2016, pp. 325–334.
doi:10.1016/j.actaastro.2016.09.023

[37] Christiansen, E. L., Cykowski, E., and Ortega, J., "Highly Oblique Impacts into Thick and Thin Targets," *International Journal of Impact Engineering*, Vol. 14, Nos. 1–4, 1993, pp. 157–168.
doi:10.1016/0734-743X(93)90017-2

[38] Neuber, H., *Theory of Notch Stress: Principles for Exact Calculation of Strength with Reference to Structural Form and Material*, 2nd ed., Springer, Berlin, 1958, pp. 20–21, 47–116.

[39] Luo, L., Xiang, Y., and Wang, Q.-Z., "Stress Concentration Factor Expression for Tension Strip with Eccentric Elliptical Hole," *Applied Mathematics and Mechanics*, Vol. 33, No. 1, 2012, pp. 117–128.
doi:10.1007/s10483-012-1537-7

R. J. Sedwick
Associate Editor